metals

MDPI

Article

Fabricating Homogeneous FeCoCrNi High-Entropy Alloys via SLM In Situ Alloying

Yaqing Hou [1,2], Hang Su [2,*], Hao Zhang [1,3], Xuandong Wang [2] and Changchang Wang [4]

[1] Central Iron and Steel Research Institute, Beijing 100081, China; houyaqing@cisri.com.cn (Y.H.); hhek@newstarteditor.com (H.Z.)
[2] China Iron and Steel Research Institute Group, Material Digital R&D Center, Beijing 100081, China; b20190575@xs.ustb.edu.cn
[3] Chongqing Adryan Technology Co., Ltd., Chongqing 401329, China
[4] Beijing Matdao Technology Co., Ltd., Beijing 100081, China; dananawang@gmail.com
* Correspondence: suhang@cisri.com.cn; Tel.: +86-1350-115-4945

Abstract: Selective laser melting (SLM) in situ alloying is an effective way to design and fabricate novel materials in which the elemental powder is adopted as the raw material and micro-areas of elemental powder blend are alloyed synchronously in the forming process of selective laser melting (SLM). The pre-alloying process of preparation of raw material powder can be left out, and a batch of bulk samples can be prepared via the technology combined with quantitative powder mixing and feeding. The technique can be applied to high-throughput sample preparation to efficiently obtain a microstructure and performance data for material design. In the present work, bulk equiatomic FeCoCrNi high-entropy alloys with different processing parameters were fabricated via laser in situ alloying. Finite element simulation and CALPHAD calculation were used to determine the appropriate SLM and post-heating parameters. SEM (scanning electron microscope), EDS (energy dispersive spectroscopy), XRD (X-ray diffraction), and mechanical testing were used to characterize the composition, microstructure, and mechanical properties of as-printed and post-heat-treated samples. The experimental results show that the composition deviation of laser in situ alloying samples could be controlled within 20 wt %. The crystal structure of as-printed samples is a single-phase face-centered cubic (FCC), which is the same as those prepared by the traditional method. The mechanical properties of the samples prepared by laser in situ alloying with elemental powder blend are comparable to those prepared by pre-alloying powder and much higher than those prepared by the traditional method (arc melting). As-printed samples can get a homogeneous microstructure under the optimal laser in situ alloying process combined with post-heat treatment at 1200 °C for 20 h.

Keywords: high-entropy alloys; laser in situ alloying; high-throughput synthesis; selective laser melting; CALPHAD; additive manufacturing

check for updates

Citation: Hou, Y.; Su, H.; Zhang, H.; Wang, X.; Wang, C. Fabricating Homogeneous FeCoCrNi High-Entropy Alloys via SLM In Situ Alloying. *Metals* **2021**, *11*, 942. https://doi.org/10.3390/met11060942

Academic Editor: Jiro Kitagawa

Received: 9 May 2021
Accepted: 5 June 2021
Published: 10 June 2021

Publisher's Note: MDPI stays neutral with regard to jurisdictional claims in published maps and institutional affiliations.

Copyright: © 2021 by the authors. Licensee MDPI, Basel, Switzerland. This article is an open access article distributed under the terms and conditions of the Creative Commons Attribution (CC BY) license (https://creativecommons.org/licenses/by/4.0/).

1. Introduction

Most structural metallic materials are based on a primary element to improve the overall performance by mixing the primary element with other elements. The pioneering work of Cantor and Yeh et al. [1,2] on mixing multiple high concentration elements has opened up a new field in material science called high-entropy alloys (HEAs). HEAs usually contain five or more major elements with a concentration between 5 and 35 at %, which have superior high temperature strength, wear resistance, and oxidation resistance [3]. Representatives are the Co-Cr-Fe-Ni-Cu system with an FCC structure and the Al-Co-Cr-Fe-Ni system with a BCC (Body-centered cubic) structure. Traditional HEAs with an FCC structure usually have high plasticity, while the one with a BCC structure usually has high strength [4]. The definition of high-entropy alloys is proposed to have at least five main elements, but sometimes ternary CoCrNi alloy as well as quaternary CoCrFeNi

and CoCrMnNi alloys have the same or better mechanical properties as CoCrFeMnNi [5]. Especially for a CoCrFeMnNi high-entropy alloy system, its strength depends mainly on the type of elements rather than the number of elements [6]. Kuzminova et al. [7] found that the yield strength of as-printed FeCoCrNi samples at the temperature range of −150 to 300 °C was twice as high as that of traditional manufactured ones. Tsau et al. found that the corrosion resistance of FeCoCrNi samples in H_2SO_4 solution prepared by arc melting was better than that of 304 stainless steel [8]. Torbati-Sarraf et al. [9] proved that the corrosion resistance of FeCoCrNi samples prepared by vacuum induction melting were better than that of FeCoCrNiMn alloy. The preparation methods of bulk HEAs mainly include vacuum melting, powder metallurgy, and additive manufacturing (AM). Vacuum melting is the most commonly used method for the preparation of HEAs [10]. Additive manufacturing of HEAs has many advantages that traditional methods do not have [11], such as precision forming of a complex structure, grain refinement of microstructure, and performance regulation of multiple process parameters. The preparation process of HEAs by AM can be divided into two categories, one is the laser cladding deposition based on powder feeding or wire feeding, and the other one is the selected laser melting (SLM) based on powder paving [12,13]. SLM is one of the hot technologies in the field of metal additive manufacturing in recent years [14]. The density of samples prepared by the SLM process could be close to the theoretical one, and the mechanical properties can be between casting and forging parts. However, the raw material powder recommended by SLM should have high purity and high sphericity. The particle size of pre-alloyed powder using SLM is usually distributed from 15 to 53 μm. Therefore, powder preparation needs to start from traditional alloying to powder atomization. Especially for the novel material, the preparation process of powder has both a long cycle and high cost. The problem of producing novel material powder is one of the factors restricting the development of SLM.

SLM in situ alloying technology involves using pure elemental powder blend for SLM, completing elements alloying directly in the process of printing and forming several high-density bulk samples. The technology can avoid the pre-alloying process of raw powder. If the powder can be mixed quantitatively in real time, high-throughput preparation of bulk samples with a combination of composition and process can be realized by the method so as to efficiently explore the innovative genes of material design. In the past, a few scholars [15,16] have used this technique to prepare shape memory alloys and refractory alloys. Due to the unique composition design idea of HEAs, the technique has gradually attracted the attention of scholars recently. However, subject to the raw material supply process of SLM, most studies are based on laser cladding deposition technology. Hasse et al. [17] printed a bulk CoCrFeMnNi sample with a size of 20 mm × 20 mm × 20 mm using mechanical mixed elemental powders by laser cladding technology. Both the strength (260 MPA) and hardness (195 HV) of the printed sample were higher than that prepared by conventional casting. By optimizing a CALPHAD database of the Co-Cr-Fe-Mn-Ni five element system, the phase composition of the system was calculated, and the distribution of elements in the solidification process was further studied. Li et al. [18] prepared a sample library of $Al_xCoCrFeNi$ (x = 0.15−1.32) alloy rapidly with 21 components by injecting Al powder on the CoCrFeNi substrate. The samples were remelted two times to improve the composition homogenization of the molten pool. Through SEM and EBSD analysis, it was observed that most of the samples presented cellular microstructures that were very similar to the cast material. With the increase of Al content, the hardness of the samples rose, and the crystalline structure of the matrix phase changed from a mixture of disordered FCC and BCC to ordered BCC. The grain size of the samples showed a power-law relationship with the cooling rate, and microstructural refinement results in increasing microhardness following a Hall–Petch relationship. Chen et al. [19] prepared bulk samples of five-element HEAs via SLM technology by mixing pre-alloyed FeCoCrNi HEAs powder with pure manganese powder mechanically. XRD analysis results showed that the as-printed samples had a single-phase FCC structure, which proved that the elemental manganese has alloyed and is distributed

homogeneously with the laser energy of 259 J/mm^3. One of the core issues of the laser in situ alloying technique is the composition homogenization of samples during rapid melting and solidification, which directly affects the microstructure and final mechanical properties of the sample. In our previous study [20], the influence law of the laser in situ alloying process and heat treatment on the composition homogenization of Fe-Ni binary alloys was calculated by the CALPHAD method. Four groups of samples with different compositions were fabricated by SLM in situ alloying, and the average density was up to 99.8%. After high temperature heat treatment at 1200 °C or 1400 °C, the laser melting pool in the samples disappeared, grains with obvious boundaries presented in the samples, and the elements were distributed basically uniformly in the grain, which verified the feasibility of SLM in situ alloying technology.

In the present work, we fabricated quaternary equiatomic FeCoCrNi samples with different processing parameters via elemental powder blend and pre-alloyed powder, respectively. The size of molten pools was calculated by the finite element analysis method to select suitable laser in situ alloying parameters. The CALPHAD method with the TCHEA4 database were used to analyze the influence of element composition deviation on the matrix phase transformation. The modified SCHEIL model coupled with Thermo-Calc software was used to calculate the micro-segregation during the rapid solidification process. The microstructure and mechanical properties of samples synthesized by two kinds of raw material powders were compared by SEM, EDS, XRD, and a room temperature tensile experiment. To get homogeneous samples, DICTRA software, (Diffusion Module (DICTRA) Stockholm, Sweden) was used to calculate a reasonable high-temperature heat treatment schedule. The corresponding heat treatment experiments were carried out, and EDS analysis was used to verify the effect of heat treatment on element distribution. The present work provides a new method to fabricate bulk HEAs with homogeneous composition and can be applied to high-throughput synthesis technology.

2. Materials and Methods

2.1. Specimens Fabrication

The elemental powders and pre-alloyed powders used in the experiment were spherical ones prepared by vacuum atomization in which the purities were between 99.5% and 99.9%. The substrate was made of 304 L stainless steel with a thickness of 2 mm. Four kinds of elemental powders were mixed with an equiatomic ratio of 1:1:1:1 (converting to mass ratio is 25:26:23:26). To keep the powder free from contamination, a special plastic powder mixing barrel with built-in blades was printed. The barrel with powder blend was mixed at a high speed for 1.5 h to keep it fully mixed. The target element composition, elemental powder weight, and basic physical properties of the raw materials calculated by CALPHAD are shown in Table 1. The sphericity and particle size distribution of the elemental powders (Figure 1) were determined by Prox-SE scanner (Phenomworld, Eindhoven, The Netherlands) and the BetterSize2000 laser particle size analyzer (Dandong Better Co., Ltd., Dandong, China).

Table 1. Target element composition, actual powder weight, and calculated physical properties of the raw materials.

Element	Fe	Co	Cr	Ni
Target composition (at %)	25	25	25	25
Target composition (wt %)	24.76	26.13	23.07	26.04
Mixing element weight (g)	945	980	873	940
Melting temperature (°C)	1538	1493	1857	1453
Boiling temperature (°C)	2750	2870	2672	2732
Room temperature density (g/cm^3)	7.87	8.90	7.19	8.91

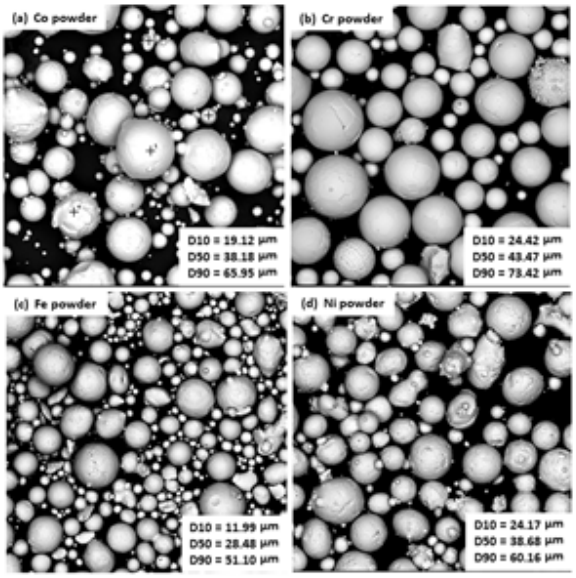


Figure 1. SEM (scanning electron microscope) image and particle size distribution of elemental powder. (**a**) cobalt powder (**b**) chromium powder (**c**) iron powder (**d**) nickel powder.

SLM-DLM280 equipment produced by Hangzhou DeDi Intelligent Technology Co., Ltd. (Hangzhou, China) was adopted to print samples. The thickness of powder layer was set to 20 μm, the scanning line spacing was 80 μm, the laser spot diameter was 80 μm, and the scanning path adopted the reverse scanning strategy, in which the scanning path between layers is perpendicular. The laser molten pool shape and size under different printing process parameters were calculated with ANSYS additive software (2020R2, Ansys Inc., Pittsburgh, PA, USA) to explore a better processing parameter scope. The designed laser power varied from 100 to 250 W, while the scanning speed varied from 700 to 1100 mm/s. The final printing process parameters are shown in Table 2, in which elemental powder samples were indicated as HEE and pre-alloyed powder samples were indicated as HEA. In the process of SLM, powders were melted with extremely high temperature and then solidified rapidly (10^4–10^5 °C/s) [21]; the microstructure and forming property of the samples were under the influence of various parameters, mainly including laser power (P, W), layer thickness (h, mm), scanning velocity (v, mm/s), and hatch spacing (s, mm), etc. For comprehensive evaluation of the forming property and comparability with reported data, volume laser energy density ($VE = P/v{\cdot}s{\cdot}h$, J/mm^3) was adopted as the evaluation criteria of laser input in this article.

Table 2. Selective laser melting (SLM) process parameters and sample labels. *VE*: volume laser density. HEA: pre-alloyed powder samples. HEE: elemental powder samples.

Sample No.	*VE* (J/mm^3)	Laser Power (W)	Scan Speed (mm/s)
HEA1, HEE1	223.21	250	700
HEA2, HEE2	178.57	200	700
HEA3, HEE3	133.93	150	700
HEA4, HEE4	89.29	100	700
HEA5, HEE5	173.61	250	900
HEA6, HEE6	138.89	200	900
HEA7, HEE7	104.17	150	900
HEA8, HEE8	69.44	100	900
HEA9, HEE9	142.05	250	1100
HEA10, HEE10	113.64	200	1100
HEA11, HEE11	85.23	150	1100
HEA12, HEE12	56.82	100	1100

2.2. Testing Methods

As-printed samples were separated from the substrate by linear cutting, and the density after cleaning and drying the samples was measured by Archimedes' drainage method. Each sample was measured two times, and the average value was taken. The macrostructure was observed by an Olympus X53 optical microscope (Olympus China Co., Ltd., Shanghai, China). The microstructure and morphology were investigated with a scanning electron microscope of Phenom ProX-SE desktop (Phenomworld, Eindhoven, the Netherlands). The composition mapping of the as-printed and heat-treatment samples was characterized by EDS simultaneously. Phase analysis of as-printed specimens was performed with a Bruker D8 Advance X-ray Diffractometer (Bruker Corporation, Billerica, Massachusetts, USA) using Co−K_α (wavelength λ = 1.7902 Å). Hardness was measured using a VH-5 Vickers Hardness indenter (Everyone Instrument Co. Ltd., Shanghai, China) with a 500 g load for 10 s. The average hardness of each specimen was evaluated from 12 to 16 measurements. Specimens of non-standard sheets were used for tensile testing, as shown in Figure 3. To make the forming at one time, the specimens were printed with a size of 2 mm × 7 mm × 80 mm. The tensile testing temperature is 20 °C, and the elongation rate is 0.05 mm/s.

2.3. Thermodynamic Calculations

Thermo-Calc software (2021, Thermo-Calc Software AB, Stockholm, Sweden) and its associated TCHEA4 database were used for phase diagram calculation, the matrix phase structure and stable temperature range were analyzed, and the calculated phase structure was compared with XRD characterization. The Scheil–Gulliver solidification model is a commonly used computational model to evaluate microstructure segregation during the rapid solidification process [21]. The model assumes that the components in the system are homogeneously mixed in the liquid and there is no diffusion in the solid phase [22]. Those conditions do not exist in nature, so the result value is a theoretical limit. In the process of actual printing, mutual diffusion of the liquid phase and solid phase will lead to a redistribution of elements, which is expected to be less than the predicted segregation value of the Scheil–Gulliver model. This work adopted a revised Scheil back diffusion model embedded in Thermo-Calc software. The model considered the diffusion of interstitial atoms between liquid and solid phase and mutual diffusion among solid phases [23]. A more accurate prediction of alloying elements segregation in the solidification process of SLM can be worked out. The segregation results were coupled with DICTRA software to serve as initial composition before homogenization heat treatment. The distance of the DICTRA diffusion model was set to 100 μm, which is the sum of two particle sizes in diameter, the composition change was step type, which on the left side of 50 μm was set to the Scheil back diffusion calculation result and on the right side of 50 μm was set to the target composition. The temperature of homogenization heat treatment ranged from 1000 to 1400 °C, maintaining time ranged from 4 to 24 h. The degree of homogenization was represented by the mean value of the standard deviation of each element within the diffusion distance.

3. Results and Analysis

3.1. Forming Performance

Powder with high sphericity has better fluidity [24], which has an important influence on the powder mixing and distributing uniformly during the SLM process. Therefore, the sphericity and particle size of pure elemental powder were analyzed by backscattering scanning, as shown in Figure 1. The average particle size of four kinds of powders was 37.2 μm, and there are also a few large particles (>53 μm). As shown in Figure 1b, the average particle size of Cr powder was the largest, and that of powders above 10% was higher than 73 μm. The average particle size of Fe powder was the smallest; however, it had a low sphericity.

The molten pool shape with different laser parameters was calculated by ANSYS additive science module, and the calculation results are shown in Figure 2. Considering the metallurgical bonding of different elements, the molten pool depth should penetrate at least 1.5 layers thickness (30 μm), and the molten pool width should cover at least the spacing hatch (80 μm). Thermophysical parameters of materials are evitable to get accurate calculation results. Therefore, Thermo-Calc software was used to calculate the average thermal expansion coefficient of the alloy as 1.65×10^{-5} K^{-1}. The chamber gas convection coefficient was set to 12.5, and the powder bulk density was set to 0.6 from the database coupled in ANSYS Additive software. The calculation results showed that when the scanning speed varied from 700 to 1100 mm/s and the laser power varied from 100 to 250 W, both the calculated depth and width of molten pools meet the forming requirements.

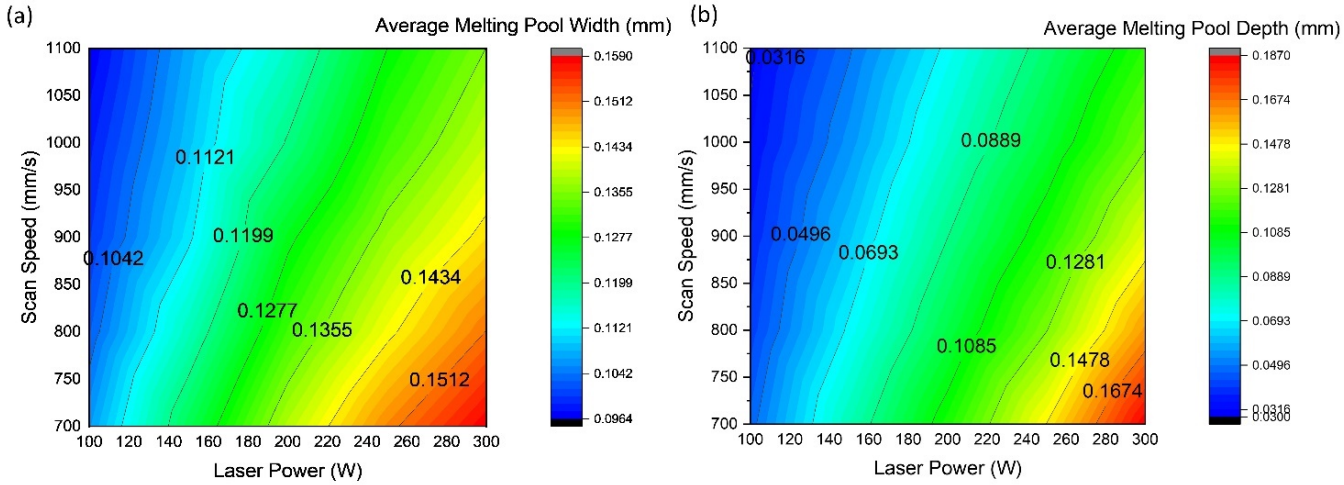


Figure 2. Calculated molten pool shape value via ANSYS Additive module: (**a**) average molten pool width, (**b**) average molten pool depth.

Twenty-four cubes with 10 mm × 10 mm × 7 mm, 9 square bars with 7 mm × 7 mm × 80 mm, 12 sheets with 2 mm × 7 mm × 80 mm, and 1 block with 20 mm × 20 mm × 7 mm were fabricated at one time. The elemental powder and pre-alloying powder were printed separately. All the samples were well formed with good surface quality, as shown in Figure 3. As-printed samples under different printing processes had no visible defects such as pores, cracks, or lack of fusion. The density measurement results of as-printed samples are shown in Figure 4, in which the relative densities are all above 98%. The density of elemental powder samples increased significantly with the increased laser energy from 56 to 104 J/mm^3, in which the maximum point is 8.06 g/cm^3 (VE = 104 J/mm^3). The maximum density of pre-alloyed samples was 8.15 g/cm^3 (VE = 89 J/mm^3), and the value fluctuated slightly around 8.1 g/cm^3 with VE varied between 56 and 220 J/mm^3, which was compatible with the experimental data from Chen Peng et al. [19]. In general, the density of laser in situ alloying FeCoCrNi samples was slightly lower than that of traditional pre-alloyed ones under the same SLM parameters. The density of elemental powder samples would decrease sharply once the energy density is lower than a certain threshold. High-density samples fabricated via elemental powder required a higher laser energy input than the pre-alloyed ones.

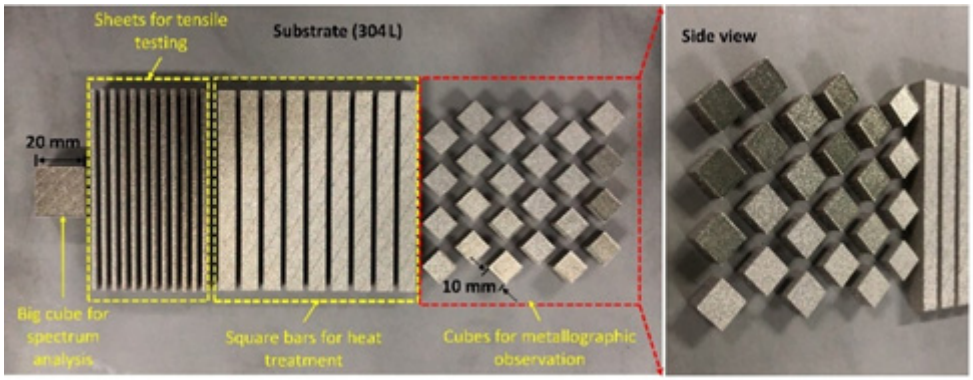


Figure 3. Optical image of as-printed samples via laser in situ alloying.

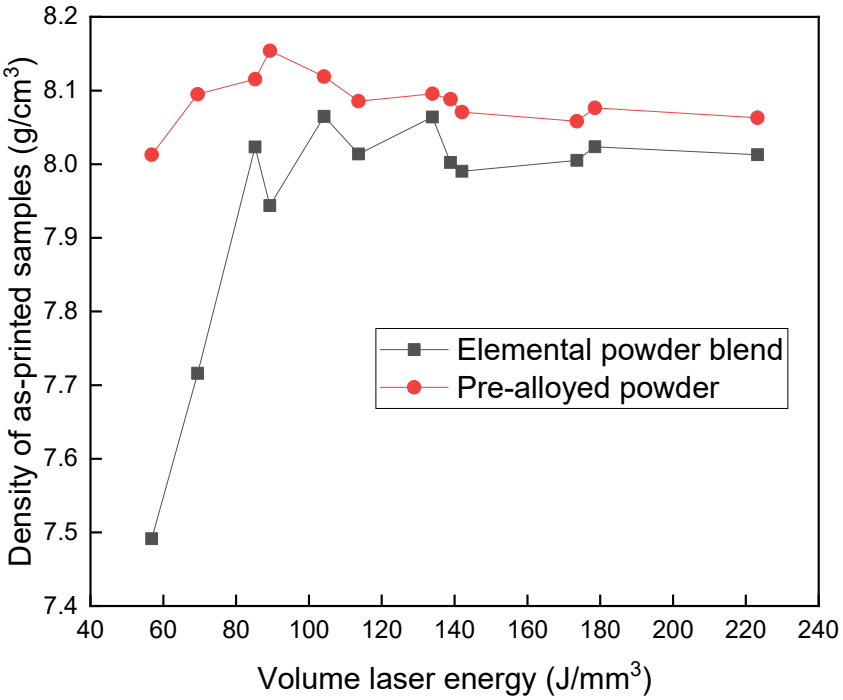


Figure 4. Density variation of as-printed samples.

3.2. Microstructure Characterization

The metallographic graph (50×) of the XY plane (perpendicular to the printing direction) of the as-printed samples fabricated via an elemental powder blend is shown in Figure 5. It can be seen from the figure that the defects such as lack of fusion gradually increased with the decrease of *VE*. When the laser energy increased above 104 J/mm^3, the number of holes basically stayed the same, which was a variation trend that is compatible with the density. A balling phenomenon occurred in the metallographic structure of samples with low energy density. Ruidi Li et al. [16] also observed the same phenomenon from SLM in situ alloying W-10%Cu powders at low energy input density. They also proposed that the spheroidizing circle was the composition gradient path formed by the lack of diffusing in time. The defeats will deteriorate the mechanical performance of samples, so the laser energy for in situ alloying FeCoNiCr alloy should be higher than 104 J/mm^3.

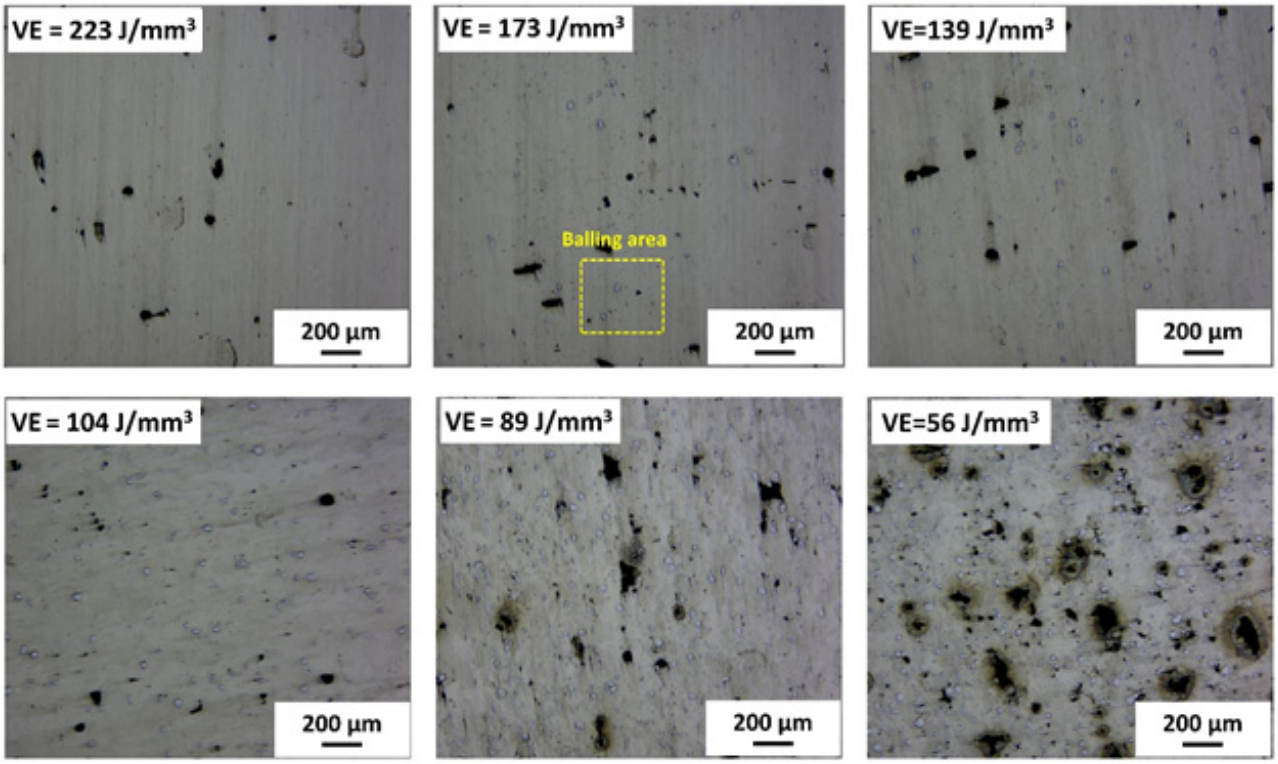


Figure 5. Metallographic images (50×) of XY surface (perpendicular to the printing direction) of as-printed samples fabricated via elemental powder blend.

The microstructure and composition mapping results on the XZ plane (parallel to the printing direction) of elemental powder samples with a magnification of 350× are shown in Figure 6. The molten pool shape of the samples with the maximum laser energy input (223 J/mm^3) were equal in size, and the boundaries were clearly visible, as shown in Figure 6a. Obvious spheroidal areas appeared in the scanning region when *VE* was reduced to 173 J/mm^3 (Figure 6b), and the depth of the molten pool also decreased. The results of energy spectrum scanning of those spheroidal areas are shown in Figure 6e. The random distribution of the spherical areas featured pure Cr-rich zones. When *VE* (Figure 6c,d) went down further, the depth of the molten pool decreased synchronously, the molten pool boundary gradually became blurred, and the Cr-rich zones that were mainly distributed in the laps between molten pools increased greatly. The boundaries between the Cr-rich zones and matrix were well fused, and there was no hole or lack of fusion. Further element composition scanning and microstructure observation of HEE1 samples are shown in Figure 7a. Except for a few occasional Cr-rich zones, other elements were homogeneously distributed. Four micro-areas of about 0.3 mm × 0.3 mm were randomly selected on the XZ plane for composition line scanning. The average value of the diagonal scanning data of micro-areas is used to characterize the average element composition. The results are shown in Table 3. Compared with the target components, the average deviation value of Fe and Co elements from the target components is only 2%, while the deviation value of Cr and Ni elements is less than 13%. The micro-area was scanned parallel to the printing direction with a length of about 260 µm, as shown in Figure 7b. Significant composition fluctuations between layers can be observed. The HEE5 sample (*VE* = 173 J/mm^3) was characterized in the same way as the results shown in Table 3. Due to the decrease of laser energy density, growing pure Cr-rich regions appeared in the sample, and the maximum element composition deviated to 17%. Semi-quantitative composition analysis of HEE7 (*VE* = 104 J/mm^3) by spark spectroscopy showed that the deviation of the highest element composition in the radius of 3 mm was less than 20%.

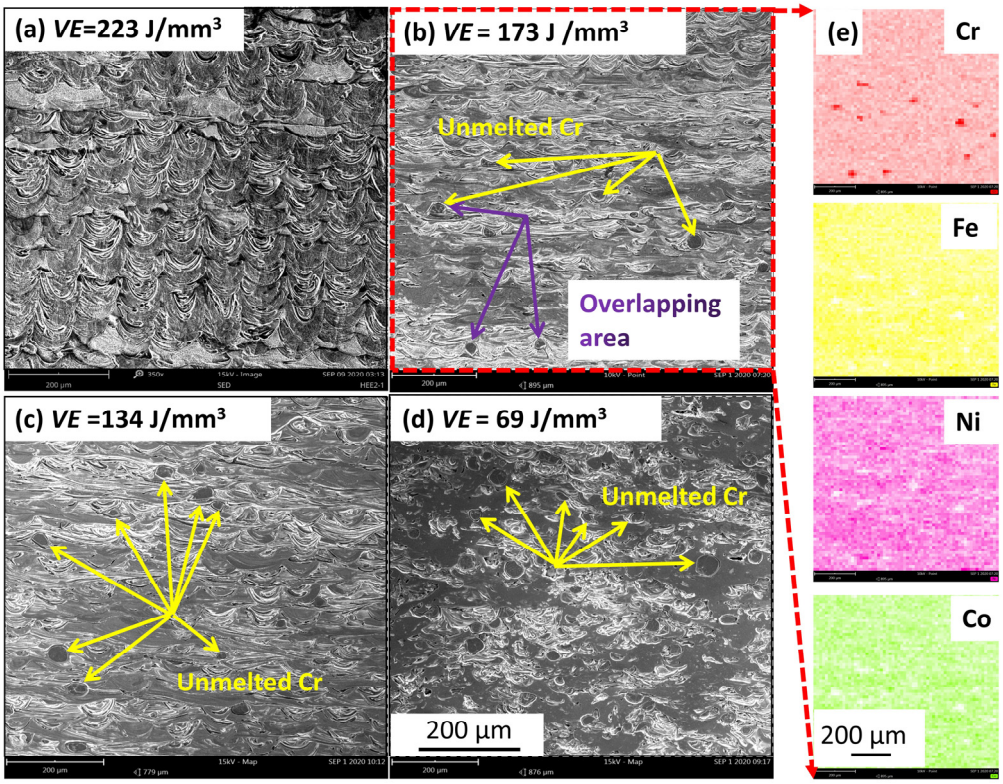


Figure 6. Microstructure and composition mapping on the XZ plane (parallel to the printing direction) of laser in situ alloying samples with a magnification of 350×: (**a**) VE = 223 J/mm^3, (**b**) VE = 173 J/mm^3, (**c**) VE = 134 J/mm^3, (**d**) VE = 69 J/mm^3, and (**e**) energy spectrum scan results of region (**a**).

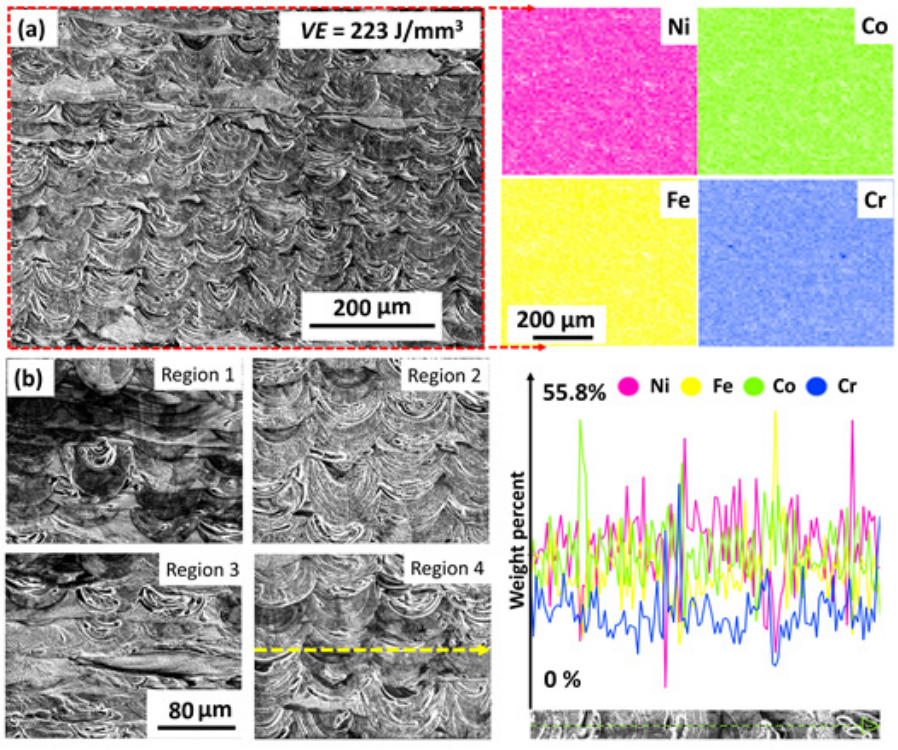


Figure 7. SEM image and EDS (energy dispersive spectroscopy) scanning results of HEE1 (elemental powder sample): (**a**) EDS scanning map, (**b**) four microregion morphologies and EDS scanning line result.

Table 3. Chemical composition of as-printed samples using EDS (energy dispersive spectroscopy) line scanning and spark spectrum.

Sample No.	Element Composition (wt %)		Fe	Co	Cr	Ni
-	Target		24.76	26.13	23.07	26.04
HEE1	EDS	Region 1	25.5	26.28	19.21	29
		Region 2	25.29	24.46	20.07	29.55
		Region 3	24.99	25.27	20.88	28.86
		Region 4	25.3	26.13	20.34	28.23
	Deviation		0.02	−0.02	−0.13	0.11
HEE5	EDS	Region 1	25.5	22.94	20.96	30.3
		Region 2	26.73	21.99	19.93	31.34
		Region 3	27.31	22.55	21.15	29
		Region 4	27.34	22.47	19.22	30.96
	Deviation		0.08	−0.14	−0.12	0.17
HEE7	Spark spectrum		20.74	29.06	20.93	29
	Deviation		−0.16	+0.11	−0.09	+0.11

Note: Deviation equal to (EDS line scan (or spark spectrum)−Target)/Target.

The phase diagram of FeCoCrNi equiatomic HEAs was calculated by Thermo-Calc software, as shown in Figure 8. The melting point of the homogeneous solid was about 1450 °C, while the single-phase FCC solid solution can be formed in the temperature range of 700–1400 °C. When the components of Fe, Co, and Cr deviated in the range of 0–20%, the matrix phase structure remained FCC unchanged, and the sigma phase precipitated in the matrix phase as the temperature went down. The matrix phase changed from a single-phase FCC structure to a two-phase FCC + BCC structure when the mass percentage of element Ni was less than 3%. In general, the deviation of element composition is all within 20% according to the above composition characterization results. The matrix phase structure of the as-printed samples should be an FCC structure according to the calculated phase diagram analysis. The XRD structures of the laser in situ alloying samples and pre-alloyed powder samples were analyzed. As shown in Figure 9, the structure of the laser in situ alloying sample and the pre-alloyed sample is an FCC single phase structure, and the phase structure is consistent with that of the sample prepared by the traditional method, which proves that the four element powders have completed the micro alloying during SLM printing. The characteristics of the SLM process determine that the sample will have serious solidification segregation. When the cooling rate of the SLM printing process is 10^5 °C/s, the Scheil back diffusion calculation results of the composition segregation between the first solidified dendrite arm and the later solidified dendrite arm in the microstructure are as shown in Figure 10. FCC_L12 is the matrix phase with a crystalline structure of ordered face-centered cubic. Affected by the interdiffusion between elements, the segregation of the Cr element is the most serious (32%), followed by the Co element (16%), while the rapid solidification process has little effect on the microstructure segregation of Fe and Ni elements. The calculation results are consistent with the measured composition deviation law of the laser in situ alloying sample of elemental powder, indicating that one of the factors leading to the composition deviation is caused by the extreme unbalanced solidification process.

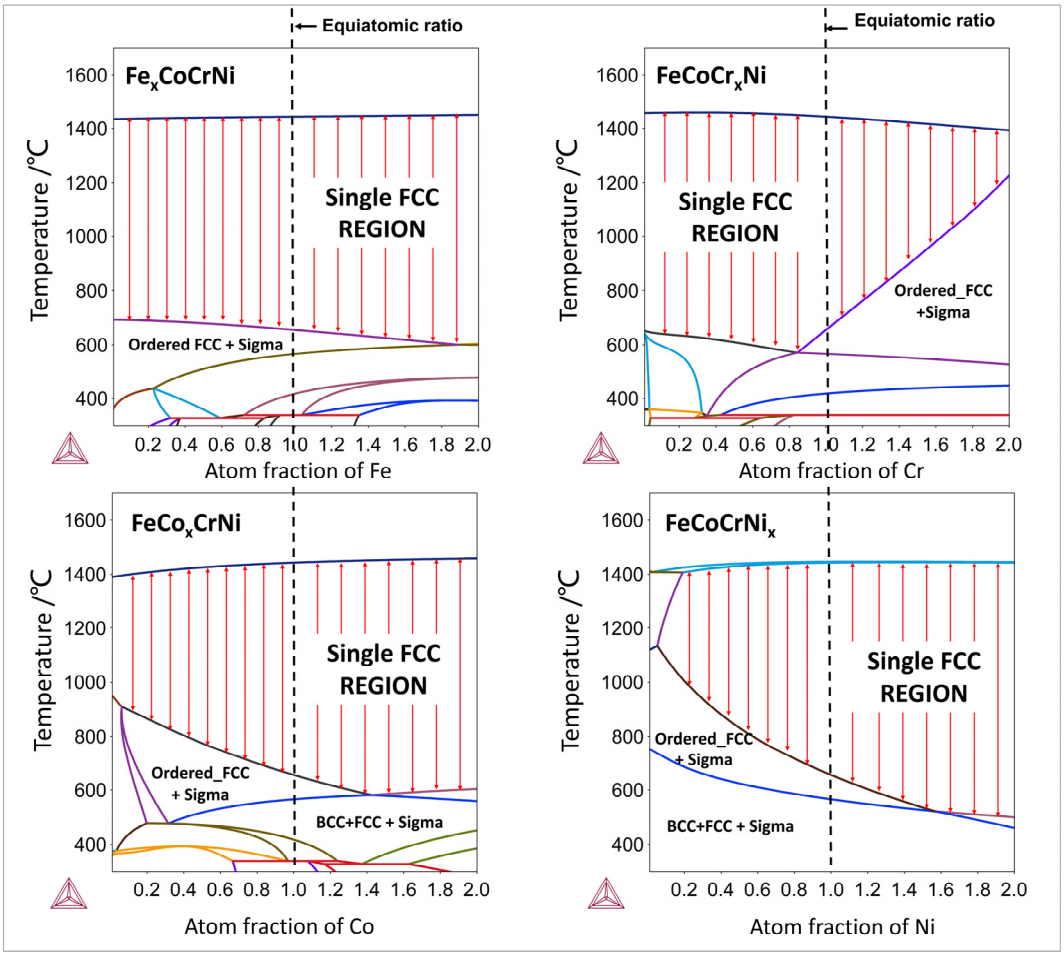


Figure 8. Calculated phase diagram of FeCoCrNi HEAs.

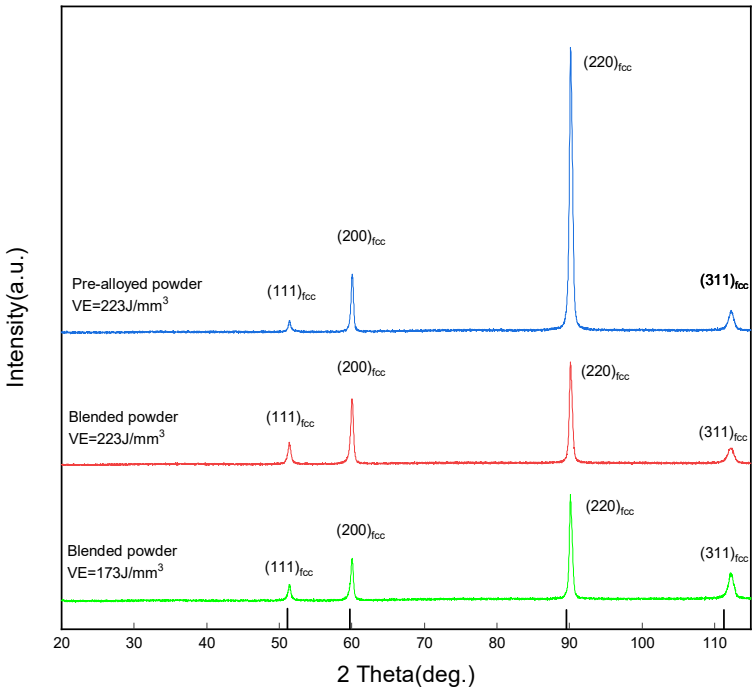


Figure 9. XRD (X-ray diffraction) patterns of as-printed samples.

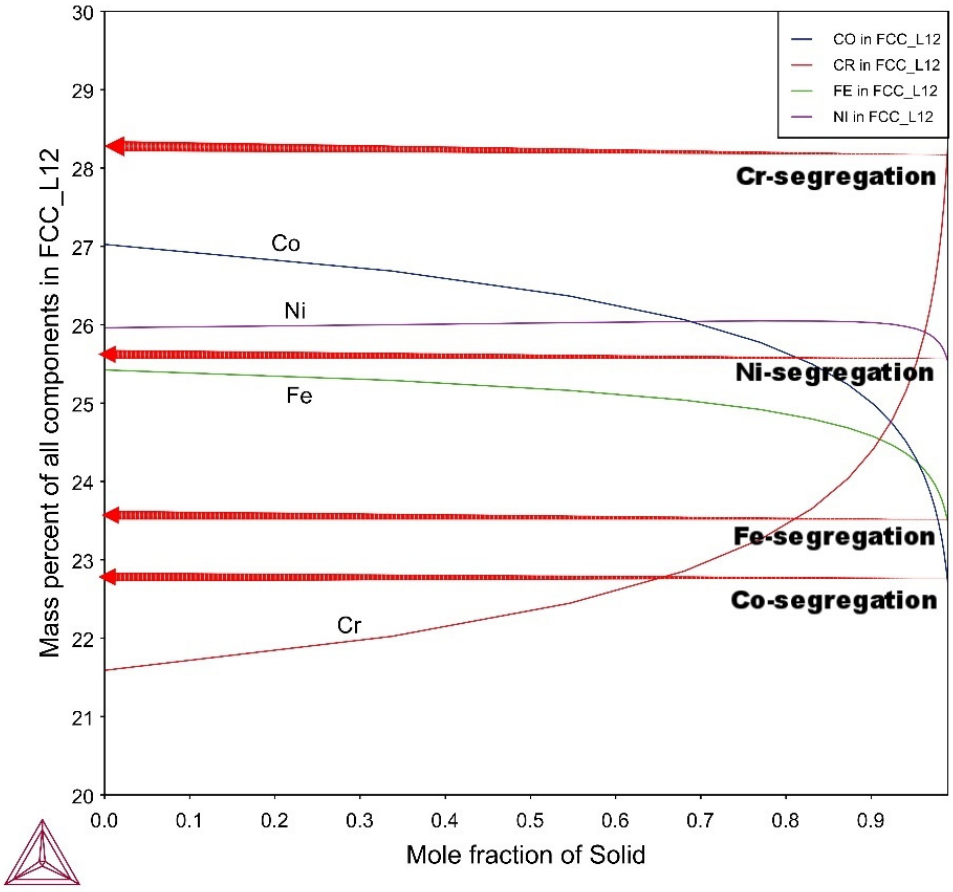


Figure 10. Calculated element segregation of as-printed samples under the solidification rate of 10^5 °C/s via the Scheil model.

Although the micro-segregation brought by the SLM process can be improved by increasing the laser power and spot diameter alongside reducing the scanning speed, it is inevitable that the subsequent high-temperature heat treatment must be combined to improve the micro-segregation. Therefore, the homogenization diffusion model built in DICTRA was used to calculate the effect of the post-heat treatment regime on element homogenization. The calculation result is shown in Figure 11. The homogenization of segregated elements could be achieved by using the heat treatment temperature of 1400 °C for a short time. The homogenization of segregated elements can be largely achieved by using the heat treatment temperature of 1200 °C for more than 12 h. There was little effect on the elements' diffusion even if the as-printed samples were under the heat treatment temperature of 1000 °C for more than 24 h. Long time and high temperature heat treatment may lead to grain boundary melting (over burning) or grain coarsening (over heating); the heat treatment schedule of 1200 °C for 20 h was selected for the experiment. The microstructure energy spectrum scanning results of the samples after heat treatment are shown in Figure 12. The elements were evenly distributed, and the grain morphology was a mixing structure of columnar grain and equiaxed grain. Therefore, the homogenization heat treatment schedule of laser in situ alloying high-entropy alloy samples can be accurately obtained by using the Scheil model coupled with the DICTRA model.

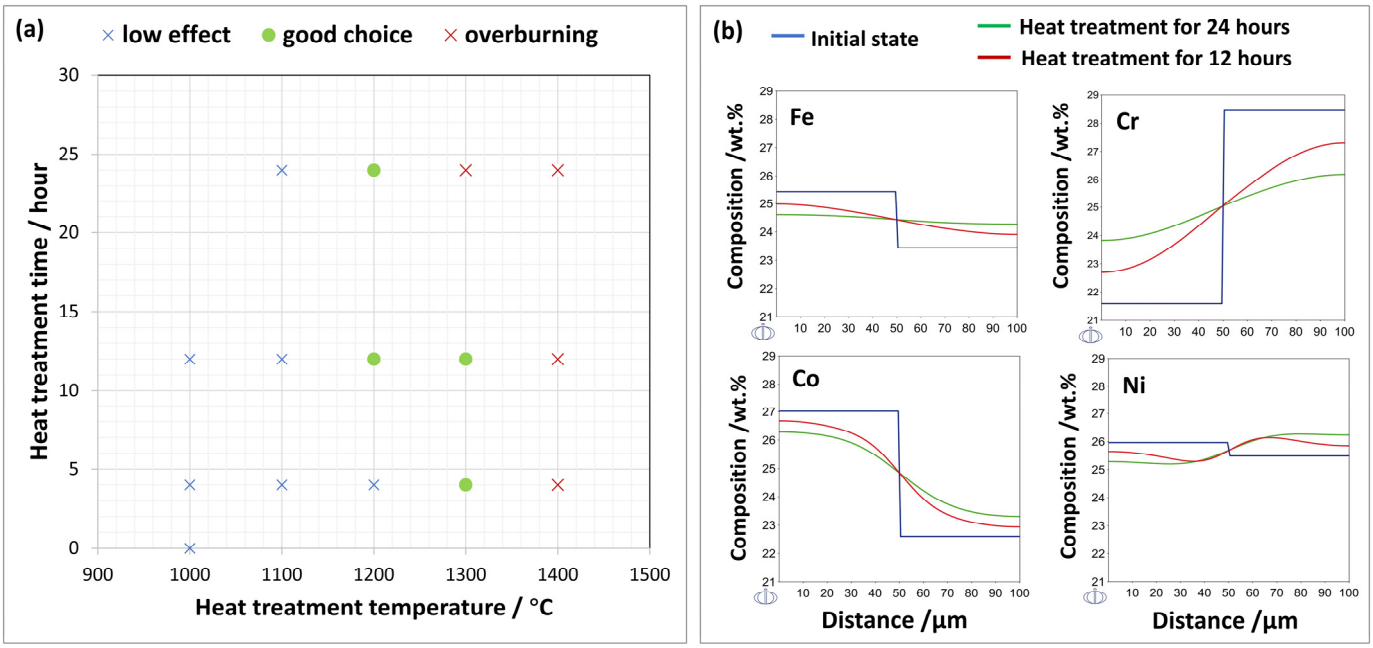


Figure 11. Calculated elements deviation after different heat treatment parameters by the Scheil back diffusion module and DICTRA software: (**a**) reasonable post-heat treatment region, (**b**) elements distribution after heat treatment of 1200 °C.

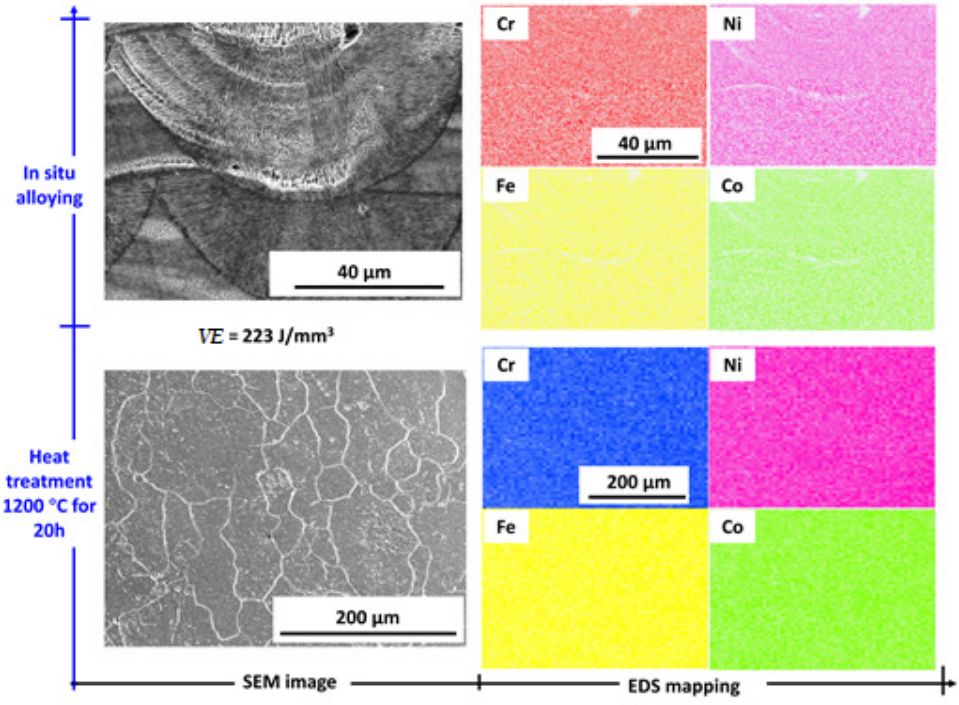


Figure 12. SEM and EDS mapping image of printed samples with elemental powder blend and post-heat-treated samples.

3.3. Mechanical Properties

The tensile strength of as-printed samples is shown in Figure 13. The strength of elemental powder samples was equal to that of pre-alloyed powder samples under the optimal energy input (140 J/mm^3). When *VE* varied between 69 and 173 J/mm^3, the tensile strength of elemental powder samples increased along with the energy density, and the value ranged from 570 to 680 MPa. The tensile strength of pre-alloy powder samples decreased with the increase of energy density, and the value ranged from 610 to 680 MPa.

The average hardness of the elemental powder samples was slightly lower than that of the pre-alloyed powder samples, as shown in Figure 14. The hardness of the elemental powder samples has no obvious correlation with energy density when it ranged from 210 to 240 HV. The hardness of the pre-alloyed powder samples increased slightly along with the energy density, which ranged from 220 to 260 HV. The comparison of mechanical properties of FeCoCrNi alloy prepared by different methods as reported in other studies in the literature are listed in Table 4. Brif et al. [25] used laser selective melting technology to print FeCoCrNi HEAs for the first time in 2015 and confirmed the printability of the alloy system. In recent years, the alloy system has also been fabricated by extrusion, rolling, and other hot working processes and obtained excellent properties [19,26–28]. According to the literature data, the strength and hardness of the elemental powder samples under an optimized process were comparable to those prepared by the pre-alloying powder and much higher than those prepared by the traditional arc melting method.

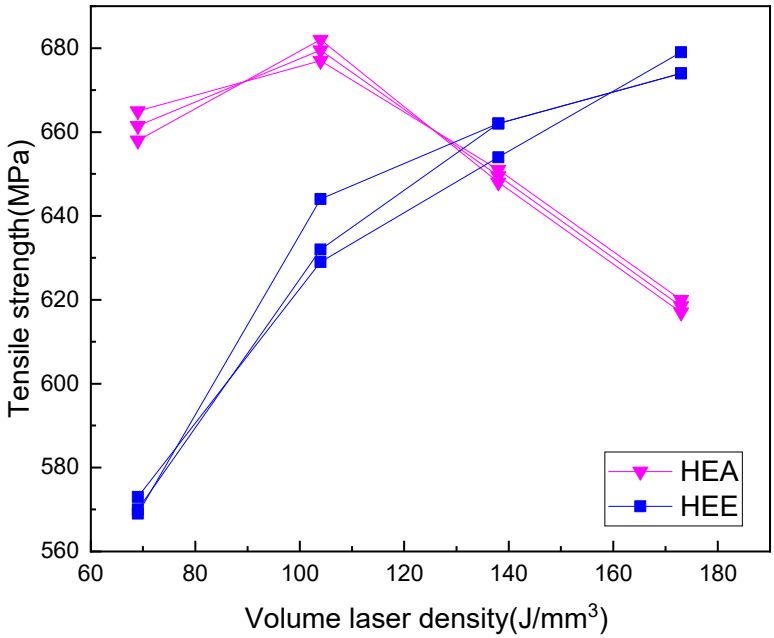


Figure 13. Tensile strength of as-printed samples with *VE* variation from 69 to 173 J/mm^3. HEA: pre-alloyed powder samples. HEE: elemental powder samples.

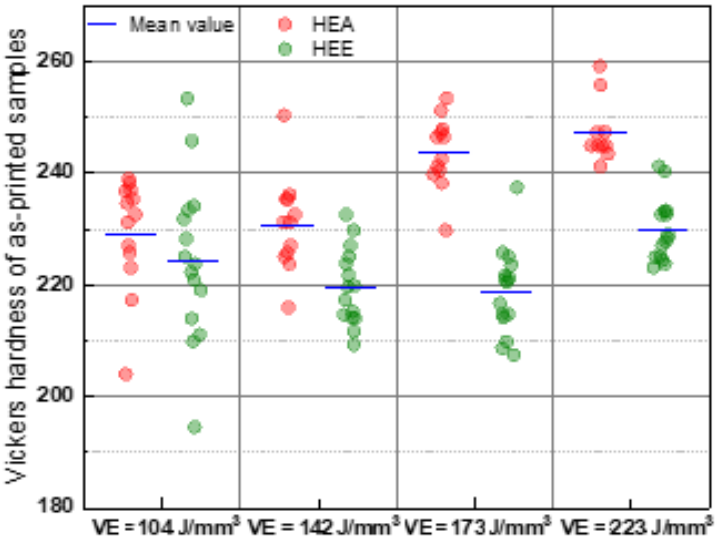


Figure 14. Vickers hardness of as-printed samples with *VE* variation from 69 to 173 J/mm^3.

Table 4. The mechanical properties of FeCoCrNi-related alloys reported in recent years.

Materials	Process	Tensile Strength (MPa)	Yield Strength (Mpa)	Elongation	Hardness (HV)	Institute
FeCoCrNi	Elemental powder blended by SLM (173.61 J/mm^3)	679	511	22.5	207	This work
FeCoCrNi	Pre-alloyed powder by SLM	745	600	32	205	Univ. of Sheffield UK [25]
	Arc melting	457	188	50	118	
FeCoCrNi	Drop casting	400	165	68	-	Univ. of Science and Technology Beijing [26]
FeCoCrNi	Casting and rolling	580	205	70.3	-	Oak Ridge National Laboratory [27]
FeCoCrNi	Powder metallurgy and extrusion	712.5	359	56	-	Central south Univ. [28]
FeCoCrNiMn	Pre-alloyed FeCoCrNi and elemental Mn powder by SLM	681 ± 14	-	12.5 ± 0.5	-	Univ. of Birmingham UK [19]
FeCoCrNiMn	Elemental powder blend by DED	-	260	-	195	RWTH Aachen Univ. [17]

4. Discussion

There were three main factors affecting the composition deviation of elemental powder samples: (1) composition deviations caused by uneven powder mixing, powder fluidity, and powder size difference during the powder laying process of SLM; (2) element segregation caused by the rapid solidification process; and (3) incomplete alloying of high melting point elements caused by insufficient laser energy density. The inhomogeneity of the powder blend in the paving process will directly lead to a great composition deviation of the final specimen from the target component. In this experiment, batch mixing powder was used, which resulted in up to 20% regional component deviation. Regional component deviation can be significantly improved if micro-zone real-time powder mixing was adopted. Serious element microstructure segregation caused by rapid melting and solidification can be eliminated by the subsequent high-temperature heat treatment.

The main reasons for the unalloyed chromium enrichment zone in the as-printed samples were as follows. (1) The melting point of Cr powder is the highest: at least 340 °C higher than other elements. (2) The average particle size of Cr powder is larger than that of other powders; more than 10% of the particle diameter is greater than 73 μm, which exceeds the recommended particle size of SLM. (3) The unalloyed zone mainly occurred in the overlap position of the molten pool, that is, the laser energy density in the heat-affected zone is not enough to realize the alloying of elements. As the scanning strategy of SLM was 80 microns hatch spacing and 80 μm laser spot diameter; that is, the overlap rate is 0, so there is a heat source blind zone at the bottom of proximate molten pools. Since the melting point of Cr is the highest, FeCoNi acted as a solution, Cr acted as a solute, and laser in situ alloying was a liquid phase sintering process. The melted FeCoNi liquid phase continuously moistened the Cr element, so the interface between the Cr-rich region and matrix was well fused, and no holes were formed. However, due to the insufficient laser energy, rapid diffusion time (only ms level), and the large particle size of the Cr powder will lead to an incomplete Cr diffusion in the liquid phase. In addition, element diffusion in the solid phase was very slow and negligible, so the Cr-rich region remained heterogeneous to room temperature after multiple thermal cycles. Overall, the alloy elements of laser in situ alloying technology should be selected as close as possible to the melting point. It is necessary to improve the laser energy density and increase the overlap rate of the molten pool in the printing process design if there is a high melting point element.

5. Conclusions

Bulk samples of FeCoCrNi equiatomic HEAs with good one-time forming performance were prepared by the SLM in situ alloying method with the processing optimization via finite element analysis and thermodynamic calculations. Combined with a real-time quantitative powder feeding device, the technology scheme can be extended to the high-throughput preparation of novel HEAs to obtain large amounts of data (composition–process–performance) for material design efficiently and quickly. The microstructure and properties of SLM in situ alloying FeCoCrNi samples via elemental powders are as follows.

(1) The SLM in situ alloying of pure elements (Fe, Co, Cr, Ni) was achieved completely within the reasonable SLM process parameter (VE = 224 J/mm^3) according to the experimental analysis and calculation results. The deviation of as-printed samples from the target composition can be controlled within 20 wt %. The matrix phase was an ordered FCC structure, which was the same with pre-alloyed powder samples. Insufficient energy, the low overlap rate of the molten pool, and the large particle size of powders led to incomplete alloying of the high melting point powder.

(2) There was a linear relationship between the density and laser energy input of elemental powder samples. It is only 1% lower than that of pre-alloyed powder samples when the energy density exceeds the critical value (VE = 224 J/mm^3). The strength and hardness of the samples were comparable to those of the pre-alloyed powder samples, which are much higher than those prepared by the traditional arc melting method. To obtain excellent performance, a higher energy input of element powder samples was required than that of pre-alloyed powder.

(3) The microstructure segregation of as-printed samples was eliminated by high-temperature heat treatment. The SHEIL + DICTRA calculation model can quantitatively give an appropriate heat treatment schedule. The calculation results show that the complete homogenization of elemental powder samples can be achieved by using the heat treatment schedule of 1400 °C for 4 h or 1200° C for 20 h. The experimental results show that homogeneous samples can be obtained by using the heat treatment temperature of 1200 °C for 20 h.

Author Contributions: H.S. performed the project administration and the analysis with constructive discussions; Y.H. contributed to the conception of the study, data analyses, and wrote the manuscript; H.Z., X.W. and C.W. helped perform the experiment. All authors have read and agreed to the published version of the manuscript.

Funding: The research was supported by the China National Key Research and Development Program (SQ2017YFGX090031).

Institutional Review Board Statement: Not applicable.

Informed Consent Statement: Not applicable.

Data Availability Statement: The data presented in this study are available on request from the corresponding author. The data are not publicly available due to potential commercial sensitivity.

Acknowledgments: This work was supported by the "Research and development of special steel for high-end equipment manufacturing industry based on rational design" project.

Conflicts of Interest: The authors declare no conflict of interest.

References

1. Yeh, J.W.; Chen, S.K.; Lin, S.J.; Gan, J.Y.; Chin, T.S.; Shun, T.T.; Tsau, C.-H.; Chang, S.-Y. Nanostructured High-Entropy Alloys with Multiple Principal Elements: Novel Alloy Design Concepts and Outcomes. *Adv. Eng. Mater.* **2004**, *6*, 299–303. [CrossRef]
2. Cantor, B.; Chang, I.T.H.; Knight, P.; Vincent, A.J.B. Microstructural development in equiatomic multicomponent alloys. *Mater. Sci. Eng. A* **2004**, *375–377*, 213–218. [CrossRef]
3. Chen, J.; Zhou, X.; Wang, W.; Liu, B.; Lv, Y.; Yang, W.; Liu, Y. A review on fundamental of high entropy alloys with promising high–temperature properties. *J. Alloys Compd.* **2018**, *760*, 15–30. [CrossRef]
4. Liu, Q.; Wang, X.; Huang, Y.; Xie, L.; Xu, Q.; Huang, J. Research Progress on High-entropy Alloy Design and Computer Simulation. *Mater. Rep.* **2019**, *33*, 392–397.

5. Miracle, D.B.; Senkov, O.N. A critical review of high entropy alloys and related concepts. *Acta Mater.* **2017**, *122*, 448–511. [CrossRef]
6. Wu, Z.; Bei, H.; Pharr, G.M.; George, E.P. Temperature dependence of the mechanical properties of equiatomic solid solution alloys with face-centered cubic crystal structures. *Acta Mater.* **2014**, *81*, 428–441. [CrossRef]
7. Kuzminova, Y.; Firsov, D.; Dudin, A.; Sergeev, S.; Zhilyaev, A.; Dyakov, A.; Evlashin, S.; Chupeeva, A.; Alekseev, A.; Martynov, D.; et al. The effect of the parameters of the powder bed fusion process on the microstructure and mechanical properties of CrFeCoNi medium-entropy alloys. *Intermetallics* **2020**, *116*, 106651. [CrossRef]
8. Tsau, C.H.; Lin, S.X.; Fang, C.H. Microstructures and corrosion behaviors of FeCoNi and CrFeCoNi equimolar alloys. *Mater. Chem. Phys.* **2017**, *186*, 534–540. [CrossRef]
9. Torbati-Sarraf, H.; Shabani, M.; Jablonski, P.D.; Pataky, G.J.; Poursaee, A. The influence of incorporation of Mn on the pitting corrosion performance of CrFeCoNi High Entropy Alloy at different temperatures. *Mater. Des.* **2019**, *184*, 108170. [CrossRef]
10. Chen, Y.X.; Zhu, S.; Wang, X.Y.; Du, W.B.; Zhang, Y. Progress in Preparation and Research of High Entropy Alloys. *J. Mater. Eng.* **2017**, *45*, 129–138.
11. Niu, P.D.; Li, R.D.; Yuan, T.C. Research Progress of High-entropy Alloys by Additive Manufacturing. *J. Netshape Form. Eng.* **2019**, *11*, 51–57.
12. Han, C.; Fang, Q.; Shi, Y.; Tor, S.B.; Chua, C.K.; Zhou, K. Recent Advances on High-Entropy Alloys for 3D Printing. *Adv. Mater.* **2020**, *32*, 1–41. [CrossRef]
13. Gao, X.; Lu, Y. Laser 3D printing of CoCrFeMnNi high-entropy alloy. *Mater. Lett.* **2019**, *236*, 77–80. [CrossRef]
14. Gunasekaran, J.; Sevvel, P.; Solomon, I.J. Metallic materials fabrication by selective laser melting: A review. *Mater. Today Proc.* **2020**, *37*, 252–256.
15. Surmeneva, M.A.; Koptyug, A.; Khrapov, D.; Ivanov, Y.F.; Mishurova, T.; Evsevleev, S.; Surmenev, R.A. In situ synthesis of a binary Ti–10at% Nb alloy by electron beam melting using a mixture of elemental niobium and titanium powders. *J. Mater. Process. Technol.* **2020**, *282*, 116646. [CrossRef]
16. Li, R.; Shi, Y.; Liu, J.; Xie, Z.; Wang, Z. Selective laser melting W-10 wt.% Cu composite powders. *Int. J. Adv. Manuf. Technol.* **2010**, *48*, 597–605. [CrossRef]
17. Haase, C.; Tang, F.; Wilms, M.B.; Weisheit, A.; Hallstedt, B. Combining thermodynamic modeling and 3D printing of elemental powder blends for high-throughput investigation of high-entropy alloys—Towards rapid alloy screening and design. *Mater. Sci. Eng. A* **2017**, *688*, 180–189. [CrossRef]
18. Li, M.; Flores, K.M. Laser processing as a high-throughput method to investigate microstructure-processing-property relationships in multi-principal element alloys. *J. Alloys Compd.* **2020**, *825*, 154025. [CrossRef]
19. Chen, P.; Li, S.; Zhou, Y.; Yan, M.; Attallah, M.M. Fabricating CoCrFeMnNi high entropy alloy via selective laser melting laser in-situ alloying. *J. Mater. Sci. Technol.* **2020**, *43*, 40–43. [CrossRef]
20. Li, C.; Hou, Y.; Su, H. Diffusion Dynamic Analysis on Selective Laser Melting Process of Fe/Ni Powder. *Mater. Rep.* **2020**, *34*, 1–5.
21. Zhang, C.; Zhu, J.; Zheng, H.; Li, H.; Liu, S.; Cheng, G.J. A Review on Microstructures and Properties of High Entropy Alloys Manufactured by Selective Laser Melting. *Int. J. Extrem. Manuf.* **2020**, *2*, 032003. [CrossRef]
22. Schaffnit, P.; Stallybrass, C.; Konrad, J.; Stein, F.; Weinberg, M. A Scheil–Gulliver model dedicated to the solidification of steel. *Calphad* **2015**, *48*, 184–188. [CrossRef]
23. Thermo-Calc Software Home Page. Available online: https://thermocalc.com/products/thermo-calc/scheil-solidification-simulations/ (accessed on 31 May 2021).
24. Ngo, T.D.; Kashani, A.; Imbalzano, G.; Nguyen, K.T.; Hui, D. Additive manufacturing (3D printing): A review of materials, methods, applications and challenges. *Compos. Part B Eng.* **2018**, *143*, 172–196. [CrossRef]
25. Brif, Y.; Thomas, M.; Todd, I. The use of high-entropy alloys in additive manufacturing. *Scr. Mater.* **2015**, *99*, 93–96. [CrossRef]
26. He, J.Y.; Wang, H.; Huang, H.L.; Xu, X.D.; Chen, M.W.; Wu, Y.; Lu, Z.P. A precipitation-hardened high-entropy alloy with outstanding tensile properties. *Acta Mater.* **2016**, *102*, 187–196. [CrossRef]
27. Gali, A.; George, E.P. Tensile properties of high- and medium-entropy alloys. *Intermetallics* **2013**, *39*, 74–78. [CrossRef]
28. Liu, B.; Wang, J.; Liu, Y.; Fang, Q.; Wu, Y.; Chen, S.; Liu, C.T. Intermetallics Microstructure and mechanical properties of equimolar FeCoCrNi high entropy alloy prepared via powder extrusion. *Intermetallics* **2016**, *75*, 25–30. [CrossRef]